Fine-scale fronts as hotspots of fish aggregation in the open ocean

Alberto Baudena[1,2], Enrico Ser-Giacomi[1], Donatella d'Onofrio[3,4], Xavier Capet[1], Cedric Cotté[1], Yves Cherel[5], and Francesco d'Ovidio[1]

[1] Sorbonne Université, CNRS, IRD, MNHN, Laboratoire d'Océanographie et du Climat: Expérimentations et Approches Numériques (LOCEAN-IPSL), Paris, France
[2] Sorbonne Université, Institut de la Mer de Villefranche sur mer, Laboratoire d'Océanographie de Villefranche, F-06230 Villefranche-sur-Mer, France
[3] Institute of Atmospheric Sciences and Climate, National Research Council (CNR-ISAC),Torino, Italy
[4] Copernicus Institute of Sustainable Development, Environmental Science Group, Utrecht University, The Netherlands
[5] Centre d'Etudes Biologiques de Chizé (CEBC), UMR 7372 du CNRS-La Rochelle Université, 79360 Villiers-en-Bois, France

Abstract. Oceanic Lagrangian Coherent Structures have been shown to deeply influence the distribution of primary producers and, at the other extreme of the trophic chain, top predators. However, the relationship between these structures and intermediate trophic levels is much more obscure. In this paper we address this knowledge gap by comparing acoustic measurements of mesopelagic fish concentrations to satellite-derived fine-scale Lagrangian Coherent Structures in the open ocean. The results demonstrate unambiguously that higher fish concentrations are significantly associated with stronger Lagrangian Coherent Structures, and we observe that these features represent a limiting condition for high fish concentrations. A model, specifically built for mid trophic levels with realistic parameters, provides a possible mechanism of fish aggregation, and is coherent with the observations. These results may help to integrate intermediate trophic levels in trophic models, which can ultimately support management and conservation policies.

Introduction

Marine biomass distribution is highly patchy and variable in time across the entire trophic web Bertrand et al. (2014); McManus and Woodson (2012). Discerning the factors underpinning ocean patchiness is fundamental to understand how they influence biogeochemical reactions and ecosystem stability Martin (2003); Lévy and Martin (2013). These issues are pivotal for conservation purposes Gaines et al. (2010) and for assessing the impact of climate change on the marine environment Hoegh-Guldberg and Bruno (2010).
One of the origins of the heterogeneity of the biotic fields is the dynamic nature of the ocean environments, which transforms the water masses on a large range

40 of temporal scales, including those of ecological relevance. In this regard, a spe-
41 cial role is fulfilled by the mesoscale and submesoscale McGillicuddy (2016), now
42 commonly referred to together as "fine-scales", which span a spatial range from
43 a few to hundreds of kilometers.
44 One fruitful approach for capturing the structuring effect of fine-scale dynamics
45 is the extraction of so-called Lagrangian Coherent Structures, and in particu-
46 lar Lagrangian fronts Haller (2015); Lehahn et al. (2018). Lagrangian Coherent
47 Structures (LCSs) provide several types of information regarding flow proper-
48 ties, such as the location of fronts, barriers to transport Boffetta et al. (2001),
49 or retentive and coherent regions d'Ovidio et al. (2013). One of the most com-
50 mon Lagrangian diagnostics used to determine LCSs is the Finite-size Lyapunov
51 Exponent (FSLE, d'Ovidio et al., 2004). This measures the exponential rate of
52 water parcel deformation and has maximal values over frontal regions.
53 By shaping and elongating water patches, Lagrangian Coherent Structures have
54 been demonstrated to set the frontiers of phytoplanktonic patches in terms
55 of chlorophyll concentration Lehahn et al. (2018), and even functional type
56 d'Ovidio et al. (2010). This in turn enhances contacts between different com-
57 munities, regulating plankton diversity De Monte et al. (2013).
58 More recently, advances in biologging programs provided evidence on the impact
59 of fine-scale structures on top predators behavior. The concentration of preda-
60 tors foraging efforts has been observed in the neighbourhoods of Lagrangian
61 fronts Kai et al. (2009); Scales et al. (2018). Furthermore, fronts detected by
62 Lagrangian Coherent Structures (which in the following we will call Lagrangian
63 fronts) have been observed to influence predators movements Della Penna et al.
64 (2015). This could enhance energy transfer and gain Abrahms et al. (2018).
65 However, while the influence of Lagrangian fronts has been observed on both ex-
66 tremes of the trophic chain, much less is known about mid-trophic levels. Prants
67 et al. (see in particular Prants et al., 2014) demonstrated a correlation between
68 Pacific saury catches and Lyapunov exponents, and Watson et al. (2018) found
69 that several fishery vessels track LCSs when targeting fishery spots. However,
70 these results leave some concerns about possible biases because commercial fish-
71 eries provides only punctual observations, and because they are even known to
72 use satellite images. Therefore, fishing vessels may target intentionally frontal
73 systems. Unbiased fish measurements have been instead recently used by Sato
74 et al. (2018) to analyse the relationship between a frontal system and acoustic
75 measurements in a coastal upwelling system. This allowed the authors to high-
76 light the different role played by in-shore and off-shore waters. In terms of the
77 mechanisms which can explain how fine-scale structures influence mid-trophic
78 biomass distribution, even less is known. Classical explanations are based pri-
79 marily on bottom-up mechanisms along fronts with intense upwelling Yoder et al.
80 (1994); Woodson and Litvin (2015). However, these hypothesis do not take into
81 account the necessity of a maturation time, which in the case of fish is con-
82 sistently longer than both the growth response of lower trophic levels and the
83 lifetime of the front. Neither the fish behavior is considered, despite the fact
84 that fish possess efficient sensorial and swimming capacities along the horizontal

85 (Kasumyan (2004)and Supporting Information SI.2).

86 The objective of the present study is to analyze the relationship between fine-
87 scale structures in the open ocean and mid-trophic organisms with unbiased,
88 direct observations of fish concentrations, and to propose a mechanism by which
89 fine-scales organize mid-trophic biomass.

90 This study was conducted in the subantarctic area of the southern Indian ocean.
91 The functioning of this region is mainly regulated by the Kerguelen plateau, a
92 major topographic barrier for the Antarctic Circumpolar Current (ACC). The
93 plateau enriches in iron, a limiting nutrient, the high-nutrients-low-chlorophyll
94 waters advected by the ACC. Depending on seasonal light conditions and stratifi-
95 cation of the water column, this provokes a large annual phytoplanktonic bloom,
96 which supports a rich trophic chain. This is one of the reasons for which the Ker-
97 guelen archipelago and its surrounding waters are part of one of the ten largest
98 marine protected areas in the world (http://www.mpatlas.org/).

99 In this region, the myctophids, also known as lantern fish, are one of the most
100 abundant groups of mesopelagic fish. They are also present in other oceans world-
101 wide and are thought to constitute one the largest portions of world fish biomass
102 Irigoien et al. (2014). They also represent important prey items for numerous
103 predators Cherel et al. (2010). Myctophids are reported to play a central role in
104 the carbon export to deep sea depths, and are suspected to affect the climate
105 Kwon et al. (2009). Constituting a potentially massive harvestable resource, they
106 are threatened to be exploited in the near future St. John et al. (2016). A bet-
107 ter understanding of the mechanisms regulating their biomass is thus urgently
108 needed.

109 In this paper, we relate acoustic measurements of fish concentrations and satel-
110 lite derived diagnostics. These diagnostics allow us to identify the intensity of
111 several fine scale fronts. The aim is to explore the degree to which fish distribu-
112 tion is shaped by these fine-scale features, and in particular Lagrangian fronts.
113 Our results indicate that stronger Lagrangian fronts aggregate larger quantities
114 of fish, although not all these structures are aggregation sites. We then propose
115 a simple aggregating mechanism specifically designed for fish, based on a cue
116 pursuing dynamic along the horizontal dimension. Myctophids are supposed to
117 be able to orientate and to actively swim to search for food (hypothesis discussed
118 in SI.2). They follow a gradient of a passive tracer, which is considered a proxy
119 for heterogeneously-distributed zooplankton. All the parameters values of this
120 model are set using observational data (SI.5) and none of them has been opti-
121 mized nor fitted. The predictions of such model are consistent with the observed
122 concentrations. In addition, the model provides also theoretical estimations of
123 the dominant spatio-temporal scales of aggregation.

4   Fine-scale fronts as hotspots of fish aggregation in the open ocean.
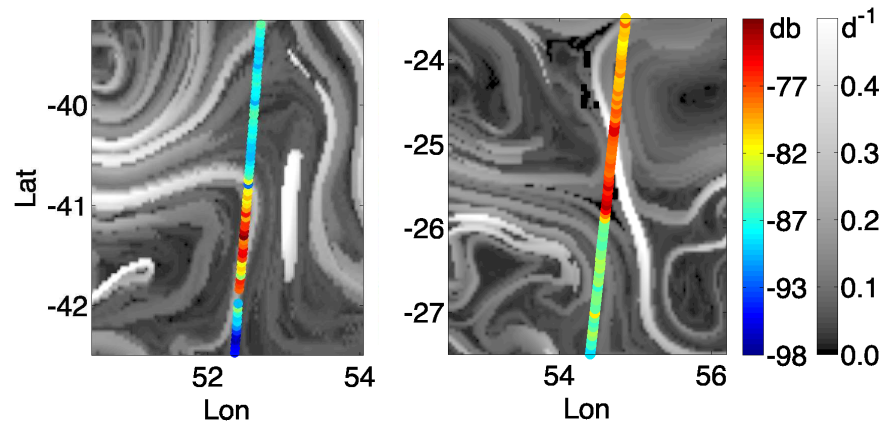

Fig. 1: Illustrative examples of two transects of the boat trajectory. The color of each dot is proportional to the Acoustic Fish Concentration (in decibels, right colorbar for scale). The transects are superimposed on a simultaneous field of Finite-size Lyapunov Exponents. These identify fine-scale frontal structures. They are computed with altimetry derived velocities (days^{-1}, left colorbar for the scale). Left panel: August, 29th, 2014. Right panel: August, 31st, 2013.

Results

Relationships between acoustic fish concentration and satellite-derived diagnostics

We used ship acoustic measurements acquired along 6 transects of 2860 linear kilometers. For each point of the boat trajectory, we computed a value of Acoustic Fish Concentration (AFC). This is representative of the fish concentration in the water column. Alongside this, we calculate two satellite derived diagnostics: the Finite-size Lyapunov Exponent (FSLE) and the Sea Surface Temperature (SST) gradient. These two metrics are typically associated with front intensity (see Materials and Methods for further details). Other diagnostics are reported in SI.1. In-situ temperature measurement were available only on a part of the transects, and were therefore not considered in the analysis.

Fig. 1 depicts two illustrative examples of the boat trajectory on August 29th, 2014 and August 31st, 2013 respectively. They are superposed on a field of Finite-size Lyapunov exponents. The latter are associated with frontal features. Each dot of the boat trajectory is colored proportionally to the AFC in that point. On both the panels, AFC values indicate a qualitative agreement with the FSLE, increasing in correspondence of the frontal features identified by high values of the Lyapunov exponents.

Fig. 2 depicts the scatter plots of the AFC against the two diagnostics, with both the axes in logarithmic scale. To determine whether the AFC values present significant differences in proximity of fine-scale features, a bootstrap analysis was conducted. Details of the methodology are provided in Materials and Methods
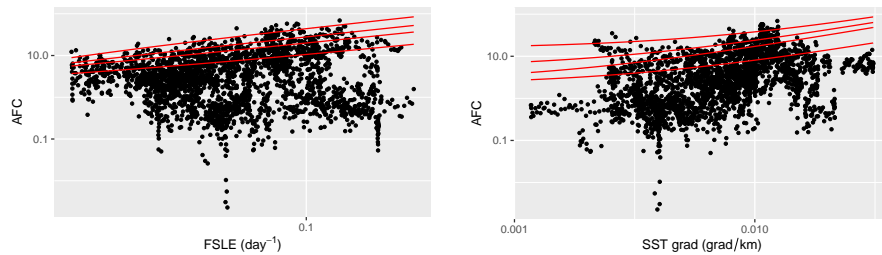
Fig. 2: Scatter plot of AFC against FSLE (left panel) and SST gradient (right panel). The lines, from the bottom to the top, indicate the linear quantile regressions at 75th, 90th, 95th and 99th percentiles. The analysis is used to investigate the relationship between the front intensity and just the higher values of fish concentration. Both axes are in logarithmic scale (values equal to zero are therefore not depicted). Values of the quantile regression coefficients are reported in Table S.1.
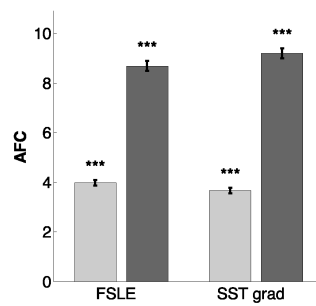
Fig. 3: Bootstrap method results. Left columns refer to FSLE analysis, right columns to SST gradient. Light gray columns represent the mean AFC under the respective threshold, and the dark gray columns represent the mean AFC over the threshold. Error bars indicate the standard deviation, while black stars indicate the significance of the bootstrap test.

section. The results are reported in Fig. 3. Significantly higher AFC values are detected over the thresholds (p-value < 0.001) for both FSLE and SST gradient.
 Finally, linear quantile regression method was employed Koenker (2005). This analysis was used to investigate the relationship between the higher values of AFC and the front intensity. Results of the regression are displayed in Fig. 2 as red lines. All the quantile slopes are statistically different from zero. This suggests the presence of a positive relationship between the higher values of AFC and FSLE and SST gradient (Table S.1).

A fine-scale mechanism of fish aggregation

Why do fish aggregate along frontal features? We addressed this question by proposing a simple mathematical model. The model assumes a gradient climb-

ing capacity, which is one of the most widespread movement mechanisms used in other biological contexts (e.g., chemotaxis, Adler (1975)). This gradient climbing capacity is specifically tuned for mid-trophic organisms and myctophids and is based on a cue pursuing dynamic. Fish try to climb a gradient of tracer. We considered this tracer a proxy of zooplankton concentration, prey of several fish species, and in particular of myctophids Pakhomov et al. (1996). At the scales considered in this study (10s of kilometers) zooplankton swimming capacities are restricted to the vertical axis Genin et al. (2005). They can thus be considered, along the horizontal axis, passive tracers. Along this dimension, zooplankton aggregation and growth is usually driven by a relatively fast response to nutrients presence, of the order of days to weeks Vidal (1980). In particular, this is valid also for zooplankton species present in our study region Alonzo et al. (2003); Labat et al. (2005). Conversely, fish have growth rates consistently slower: in particular, pelagic fishes and myctophids are considered as "slow-growing fish", with lifetimes spanning few years Greely et al. (1999). Therefore, their aggregation can not be explained by the same dynamics affecting the zooplankton. Alongside this, fish have extremely developed sensorial capacities and, differently from zooplankton, they can actively swim, with both capacities involved in many functional activities, including feeding Kasumyan (2004). These arguments support our approach of modelling zooplankton as a passive tracer and fish as active swimmers (we invite the reader to refer to SI.2 for further details). To include ocean patchiness, we perturbed the ability of the fish to properly identify the spots of zooplankton with a noise term. However, we assumed that fish are able to orientate without problems over a given threshold of the zooplankton gradient. This threshold was estimated from the zooplankton concentrations (SI.5).

Making these assumptions, the average velocity of a group of fish $U_F(x)$ can be found applying simple algebra to a standard gradient climbing model (see Materials and Methods, subsection "Gradient climbing model"):

$$U_F(x) = V \frac{\frac{\partial T}{\partial x}}{\frac{\partial T}{\partial x}_{MAX}} \left(2 - \frac{\left|\frac{\partial T}{\partial x}\right|}{\frac{\partial T}{\partial x}_{MAX}} \right) \qquad (1)$$

in which T is the zooplankton concentration, $\frac{\partial T}{\partial x}_{MAX}$ is the threshold of the zooplankton gradient, and V is the cruising speed of the myctophids.

Similarly, the evolution of the fish concentration over time can be easily obtained from the one-dimensional continuity equation, by imposing the conservation of fish total biomass, and by using Expr. 4 (see Materials and Methods for further details). The tracer shape used describes a sigmoid function, which models a generic local gradient in the zooplankton concentration. At the limits of the plateau, the tracer decreases along a distance of ∼5 km, a typical fine-scale range.

Four different snapshots (at 0, 6 hours, 1 day and 4 days) of the fish modelled concentration are illustrated in Fig. 4. Intuitively, having chosen a gradient-climbing behavior, one can expect that fish concentration will evolve quickly in the regions in which the tracer gradient is larger. Indeed, after only 6 hours,

two peaks of doubled concentration are present in correspondence with the margins of the tracer plateau. In the following days, the two peaks decreased their growth rate, while the concentration between them increases until they merged together. The fish concentration is thus homogeneous over the plateau, presenting values between 2.5 and 3.5 times higher than the initial concentration. In case of a larger plateau (Fig. 5), the model predicts a similar behavior, but the merging between the peaks occurs over longer timescales. In that case, the peaks reach their maximum value after the first day, with the creation of two regions of increased concentration at the margins of the plateau. Changing the type of fish behavior leads to similar results (see SI.3).

We note that this mechanism does not explicitly take into account fronts. However, in the oceanic environment, frontal regions represent areas of convergence of water masses with different properties. This is why regions of strong gradients are often associated to frontal features Yoder et al. (1994).

However, at the same time during which this mechanism occurs, the tracer can evolve. As a sensitivity test, we numerically analyzed a scenario in which the tracer, subjected to a typical frontal dynamics, is stretched in a filament and eroded by diffusion (SI.4). Using realistic bio-physical parameters representative of the study area, we found that these tracer dynamics do not compromise the aggregation mechanism presented above, but may even facilitate the aggregation of fish along frontal zones. Indeed, the model developed predicts several quantitative information, such as an estimate of the fish aggregation over time. The latter highlighted a final concentration, on average, an order of magnitude stronger than the initial one. In addition, it was possible to obtain the "school life time". This quantity indicates the amount of time during which a group of fish is able to follow a patch of interest before it vanishes due to the frontal
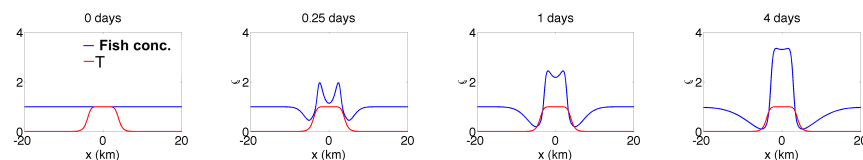

Fig. 4: Time evolution of the fish concentration (blue line, adimensional) according to the continuity equation. The tracer (red line, adimensional) describes a plateau of 8 km in width. At its limits, its values range from 1 to 0 in about 5 km. Each panel represents a different snapshot at 0, 6 hours, 1 day, and 4 days.
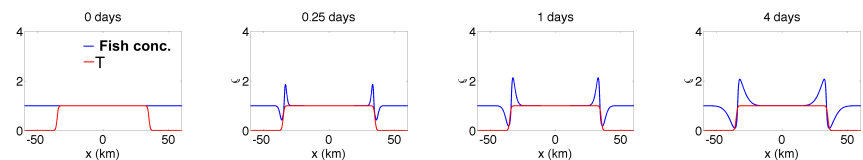

Fig. 5: Time evolution of the fish concentration as reported in Fig. 4. This time, the plateau width has been set to 70 km.

dynamics. The school life times we obtained ranged between 7 to 25 days, with an average value of around 2 weeks. Remarkably, this amount of time matches with that of fine-scale processes.

Discussion

In the oceans, patchiness characterizes biomass distribution, which regulates ecosystem stability and biogeochemical processes Bertrand et al. (2014); Martin (2003); Lévy and Martin (2013). In the open ocean, biomass distribution is largely driven by processes at the fine-scale (between 1 and hundreds of kilometers or a few days to several weeks, such as lateral advection and horizontal stirring Martin (2003); Lévy et al. (2018).
One approach to studying the structuring processing occurring at this scale is provided by Lagrangian methods. In the past, Lagrangian tools like the computation of Lagrangian Coherent Structures have revealed the structuring role of fine-scale dynamics on primary levels of the trophic chain (see a review in Lehahn et al. (2018)). On the other hand, they have highlighted their influence on apex predators behaviors as well Kai et al. (2009); Scales et al. (2018).
However, less information is available on intermediate trophic levels. In the present study (i) we correlate the intensity of acoustic fish concentrations and fine-scale fronts, and (ii) we propose a mechanism of fish aggregation along fronts. We analyze the Kerguelen region in the Southern Ocean, one of the ten largest protected areas in the world, and an oasis for several threatened species (IUCN, https://www.iucn.org/). The reference fish of this study are the myctophids, which are highly diffused in that region and one of the most abundant group of mesopelagic fish in the world Irigoien et al. (2014).
Our results reveal a significant difference in fish concentration between frontal and non-frontal features. These are difficult to explain with traditional mechanisms usually prescribed to lower trophic levels, such as rapid growth associated to a presence of nutrient, because fish have slower growth rates. Therefore, starting from a homogeneous fish distribution and applying simple ecological rules, we propose a gradient-climbing model specifically calibrated for the study of mid-trophic organisms. Once parameterized with values typical for the study region, the model demonstrates a quick response to gradient structures. Two peaks of doubled concentration appear after just 6 hours, and then merge after 4 days. Fish thus tend to be homogeneously distributed over the entire patch of interest. This is in coherence with on-going studies on myctophids' response to food concentration. These presuppose that myctophids have a Holling type III functional response, in that they ingest always the same quantity of food over a certain prey density (A. Hulley, personal communication).
Tracer patchiness is known to be associated with frontal features Yoder et al. (1994); Lehahn et al. (2018). However, patchiness evolves, and under the double effect of stretching and diffusion, local gradients can be eroded. Thus, we tested the robustness of our model to this feature in SI.4. As in the former case, none of the parameters employed has been optimized nor fitted, but they all represent

rigorous estimations of Southern Ocean physical and biological conditions, such as stretching and mixing rates or fish cruising speed. Results allowed us to estimate a typical lifetime for a fine-scale patch of around two weeks, much longer than the peak doubling time ($\sim$ 6 hours). This robustness analysis is consistent with the hypothesis of a fixed tracer assumed in the gradient climbing scenario. Furthermore, we demonstrated that the stretching and diffusion dynamics can potentially enhance fish aggregations.

The patch of interest is considered as a proxy of zooplankton concentration. However, being parameterized as a passive tracer, it can be considered, more simply, as a physical water property. Indeed, physical characteristics, such as temperature, have been proven to be used by predators to find favorable conditions where concentrated food occurs Snyder et al. (2017).

The proposed mechanism of aggregation needs two obvious initial conditions: the presence of fish, and the presence of a zooplankton patch. It is presumable that fine-scale fronts, lacking one or both these conditions, cannot act as aggregating spots. Furthermore, while we assumed that the aggregation occurs after a certain amount of time, the environment studied is dynamic. Thus, it is likely that the aggregation mechanism was observed during different stages. The statistically significant positive relationships between the high values of acoustic fish concentration with the front intensity diagnostics confirms the previous considerations. Not all of the strong fronts detected indicate high acoustic fish concentrations. On the contrary, strong fish aggregation is preconditioned by the intensity of a frontal feature. Our results suggest that fronts represent in this regard a limiting condition for high fish concentrations. Model predictions are in accordance with the observations. Furthermore, the model provided estimations of other aggregation dynamics, such as the dimensions of the aggregation patterns or its intensity, with timescales comparable with those of fine scale processes. Specific experiments are necessary to validate these outputs, which however look promising.

Within the ACC, little information available on mid-trophic levels reported that the large circumpolar fronts are known to host (i) large densities of zooplankton and myctophids and (ii) that these organisms are patchily distributed Pakhomov and Froneman (2000). We identified in this study, at least partly, the potential mechanisms driving the patchiness observed at fine-scale. Assessing the preconditions and the other dynamics necessary for front aggregation is a new, open challenge emerging from the present work.

Note that in our work we focus only on open ocean Lagrangian fronts, that is, fine-scale frontal features induced by the mesoscale open ocean activity. In particular, we intentionally exclude coastal fronts as well as large scale fronts, whose dynamics and ecological role may be different (e.g., Lara-Lopez et al. (2012); Netburn and Koslow (2018); Sato et al. (2018)). Finally, the limitations of our analysis must be discussed. No vertical dynamics has been included in the model presented. However, these play an important role in the organization of marine biota Lévy et al. (2018), and, typically, stronger gradients are present along the vertical Ohman (1988). This assumption is due to the fact that, while

knowledge on horizontal dynamics is more advanced, 3D Lagrangian analyses, while appealing Sulman et al. (2013), are not currently possible, due to a lack of quantitative information on the vertical velocities of the ocean. Future satellite missions (such as SWOT: https:/swot.cnes.fr) will possibly help to mitigate this problem, by helping the assimilation scheme to better reconstruct the three dimensional dynamics Morrow et al. (2019). At the same time, they will also improve satellite resolution, providing a more precise location of fine-scale fronts. The model studied does not consider the diel vertical migration of myctophids either. This choice is driven by the difficulty in parameterizing such a non linear behavior and in assimilating different migratory diel patterns. However, we note that many zooplankton species exhibit a diel cycle as well. Finally, zooplankton consumption due to fish foraging is considered to be negligible, or compensated by source terms (like blooms). The limitations presented can open the way for future investigations. Thus, the present study sheds some light on a largely unexplored topic.

The results presented here may be useful for improving the representation of intermediate trophic levels to coupled ecological and physical models Robinson et al. (2011), habitat models PC et al. (2018), targeting the mesopelagic compartment in particular. At the same time, the possibility of using Lagrangian Coherent Structures as a proxy of higher fish concentrations may further improve the integration of satellite-derived Lagrangian tools in conservation planning Penna et al. (2017).

Materials and Methods

Acoustic measurements

Two subsets of data were used for the analysis. Both of them were collected within the Mycto-3D-MAP program. The first subset (named MYCTO) was collected during 6 campaigns in 2013 and 2014, both in summer and in winter (see Tab. 1 for more details), using split-beam echo sounders at 38 and 120kHz. The data were then treated with a bi-frequency algorithm, applied to the 38 and 120 kHz frequencies (details of data collection and processing are provided in Béhagle et al. (2017)). This provides a quantitative estimation of the concentration of gas-bearing organisms, mostly attributed to fish containing a gas-filled swimbladder in the water column Kloser et al. (2009). Most mesopelagic fish present swimbladders and several works pointed out that myctophids are the dominant mesopelagic fish in the region Duhamel et al. (2014). Therefore, we considered the acoustic signal as mainly representative of myctophids concentration. Data were organized in acoustic units, averaging acoustic data over 1.1 km along the boat trajectory on average. Myctophid school length is in the order of tens of meters Saunders et al. (2013). For this reason, acoustic units were considered as not autocorrelated. Every acoustic unit is composed of 30 layers, ranging from from 10 to 300 meters (30 layers in total).

The second subset of data (named ZOO) was collected between January the 22nd and February the 5th, 2014. It was processed in the same manner as the

other dataset, but this time the bifrequency algorithm was used to infer the
zooplankton biomass. This second subset possesses a higher resolution with an
acoustic unit every 206 m of the boat trajectory on average.

The two datasets were used to infer the Acoustic Fish Concentration (AFC) and
the Acoustic Zooplankton Concentration (AZC) in the water column, respec-
tively. We considered as AFC (or AZC) of the point (x_i, y_i) the average of the
bifrequency acoustic backscattering on the whole column, with the exclusion of
the first layer. The latter was not considered due to surface noise.

The AZC was used to compute the zooplankton gradient. The zooplankton gra-
dient of a point i of the boat transect is computed as:

$$\frac{\partial Z}{\partial x}(i) = \frac{1}{2}\left(\frac{Z_i - Z_{i-1}}{d_{i-1}} + \frac{Z_{i+1} - Z_i}{d_i}\right)$$

in which d_i indicates the kilometric distance between the point $i + 1$ and i, and
Z_i is the cubic spline interpolation (to smooth the noise effects), in an around of
2 km, of the zooplankton concentrations. This type of interpolation, in contrast
with the moving average, preserves the trend of the data, and thus a possible
front.

Acoustic campaigns details

Cruise	Season	St. Date	End Date	Distance (km)
LOGIPEV193_RUNKER	Summer	09/02/2013	17/02/2013	2752
LOGIPEV193_KERMAU	Summer	04/03/2013	10/03/2013	3781
OP2013-2_RUNKER	Winter	30/08/2013	10/09/2013	3310
LOGIPEV197_RUNKER	Summer	06/01/2014	13/01/2014	2800
LOGIPEV197_KERMAU	Summer	06/02/2014	18/02/2014	2045
OP2014-2_RUNKER	Winter	24/08/2014	04/09/2014	3677

Table 1: Details of the acoustic transects analyzed.

Regional data selection

The geographic area of interest of the present study is the Southern Ocean. To
select the boat trajectory points belonging to this region, we used the ecopar-
tition of Sutton et al. Sutton et al. (2017). Only points falling in the *Antarctic
Southern Ocean* region were considered. We highlight that this choice is con-
sistent with the ecopartition of Koubbi et al. Koubbi et al. (2011) (group 5),
which is specifically designed for the myctophids, the reference fish of this study.
Furthermore, this choice allowed us to exclude major fronts which have been the
subject of different research works Lara-Lopez et al. (2012); Netburn and Koslow
(2018). In this way our analysis is focused specifically on fine scale fronts.

Day-night data separation

Several species of myctophids present a diel vertical migration. They live at great depths during the day (between 500 and 1000 m), ascending at dawn in the upper euphotic layer, where they spend the night. Since the maximal depth reached by our equipment is 300 m, in the analysis reported in Fig. 2 and 3 we excluded data collected during the day. However, their analysis is reported in SI.1. This is also consistent with the use of the Lagrangian and Eulerian diagnostics. These quantities, obtained from geostrophic velocity fields, are representative of the first part of the water column (~ 50 m).

Satellite data

Velocity current data and processing. Velocity currents are obtained from the Sea Surface Height (SSH), which is measured by satellite, through the geostrophic approximation. Data, which were downloaded from E.U. Copernicus Marine Environment Monitoring Service (CMEMS, http://marine.copernicus.eu/), were obtained from DUACS (Data Unification and Altimeter Combination System) delayed-time multi-mission altimeter, and displaced over a regular grid with spatial resolution of $\frac{1}{4} \times \frac{1}{4}^{\circ}$ and a temporal resolution of 1 day.
Trajectories were computed with a Runge-Kutta scheme of the 4th order with an integration time of 3 hours. Finite-size Lyapunov Exponents (FSLE) were computed following the methods in d'Ovidio et al. (2004), with initial and final separation of 0.04° and 0.4° respectively. This Lagrangian diagnostic is commonly used to identify Lagrangian Coherent Structures. This method determines the location of barriers to transport, and it is usually associated with oceanic fronts Haller (2015).
Temperature field. The Sea Surface Temperature (SST) field was downloaded from the OSTIA global foundation Sea Surface Temperature product (SST_GLO_SST_L4_NRT_OBSERVAT The data are represented over a regular grid with spatial resolution of $0.05 \times 0.05^{\circ}$ and daily-mean maps.
Satellite data extrapolation. For each point of the boat trajectory, we considered as value of the diagnostic the average value over a disc of radius σ. Different σ were tested, and the best results were obtained with the $\sigma = 0.2^{\circ}$, reference value reported in the present work. This value is consistent with the uncertainty of the satellite velocity field.

Statistical processing

Bootstrap method. In this section, we describe the analysis necessary for the bootstrap test. To identify the frontal features, the following diagnostic values were chosen as thresholds for representing the front: for the FSLEs, we used 0.08 days^{-1}, a threshold value consistent with those chosen in De Monte et al. (2012) and obtained from Kai et al. (2009). For the SST gradient, we considered representative of thermal front values greater than 0.9°C/100 km, which is about the half of the value chosen in De Monte et al. (2012). However, in that work, the

458 SST gradient was obtained from the advection of the SST field with satellite-
459 derived currents for the previous 3 days, which structures it in high resolution
460 features that therefore present higher gradient values.
461 The threshold value splits the AFC into two groups: over and under the thresh-
462 old. Their independency was tested using a Mann-Whitney or U test. Finally,
463 bootstrap analysis is applied following the methodologies used in De Monte et al.
464 (2012).
465 *Linear quantile regression.* Linear quantile regression method Koenker (2005)
466 is employed to estimate the effect of FSLE and SST gradient on the upper
467 limit of the AFC, as in Sankaran et al. (2005). The percentiles values used are
468 75th, 90th, 95th, and 99th. The analysis is performed using the statistical pack-
469 age QUANTREG in R (https://CRAN.R-project.org/package=quantreg, v.5.38,
470 Koenker (2005)), using the default settings.

Gradient climbing model

472 The fish searching dynamic is considered a one dimensional, individual-based,
473 Markovian process. Time is discretized in timesteps of length $\Delta\tau$. We presuppose
474 that, at each timestep, the fish chooses between swimming in one of the two
475 directions. This decision depends on the comparison between the quantity of
476 tracer at its actual position and the one perceived at a distance f_W from it,
477 where f_W is the field view of the fish. We consider the fish immersed in a tracer
478 whose concentration is described by the function $T(x)$.
479 An expression for the average velocity of the fish, $U_F(x)$, can now be derived.
480 We assume that the fish is able to observe simultaneously the tracer to its right
481 and its left. Fish sensorial capacities are discussed in SI.2. The tracer observed
482 is affected by a noise. Noise distribution is considered uniform, with $-\xi_{MAX} <$
483 $\xi < \xi_{MAX}$, $\xi_{MAX} > 0$. The effective values perceived by the fish, at its left and
484 its right, will be, respectively:

$$\tilde{T}(x_0 - \Delta x) = T(x_0 - \Delta x) + \xi_1$$
$$\tilde{T}(x_0 + \Delta x) = T(x_0 + \Delta x) + \xi_2 \ .$$

485 We assume that, if $\tilde{T}(x_0 + \Delta x) > \tilde{T}(x_0 - \Delta x)$, the fish will move to the right,
486 and, vice versa, to the left. We hypothesize that the observational range is small
487 enough to consider the tracer variation as linear, as illustrated in Fig. S.6 (SI.3).
488 In this way:

$$\tilde{T}(x_0 + \Delta x) = T(x_0) + f_W \frac{\partial T}{\partial x} + \xi_1$$
$$\tilde{T}(x_0 - \Delta x) = T(x_0) - f_W \frac{\partial T}{\partial x} + \xi_2 \ .$$

489 In case of absence of noise, or with $\xi_{MAX} < f_W \frac{\partial T}{\partial x}$, the fish will always move
490 in the correct direction, in that it will climb the gradient. Assuming V as the

cruising swimming velocity of the fish, this means $U_F(x) = V$.

Let's now assume $\xi_{MAX} > f_W \frac{\partial T}{\partial x}$. If $T(x_0 + \Delta x) > T(x_0 - \Delta x)$ (as in Fig. S.6), and the fish will swim leftward if

$$\xi_1 - \xi_2 > 2f_W \frac{\partial T}{\partial x} \,.$$

Since ξ_1 and ξ_2 range both between $-\xi_{MAX}$ and ξ_{MAX}, we can obtain the probability of leftward moving $P(L)$. This will be the probability that the difference between ξ_1 and ξ_2 is greater than $2f_W \frac{\partial T}{\partial x}$

$$
\begin{aligned}
P(L) &= \frac{1}{8\xi_{MAX}^2} \left(2\xi_{MAX} - 2f_W \frac{\partial T}{\partial x} \right)^2 \\
&= \frac{1}{2} \left(1 - \frac{f_W}{\xi_{MAX}} \frac{\partial T}{\partial x} \right)^2
\end{aligned}
$$

The probability of moving right will be

$$P(R) = 1 - P(L)$$

and their difference gives the frequency of rightward moving

$$
\begin{aligned}
P(R) - P(L) &= 1 - 2P(L) = 1 - \left(1 - \frac{f_W}{\xi_{MAX}} \frac{\partial T}{\partial x} \right)^2 \\
&= \frac{f_W}{\xi_{MAX}} \frac{\partial T}{\partial x} \left(2 - \frac{f_W}{\xi_{MAX}} \left| \frac{\partial T}{\partial x} \right| \right) \,,
\end{aligned}
$$

where the absolute value of $\frac{\partial T}{\partial x}$ has been added to preserve the correct climbing direction in case of negative gradient. The above expression leads to:

$$U_F(x) = \frac{V f_W}{\xi_{MAX}} \frac{\partial T}{\partial x} \left(2 - \frac{f_W}{\xi_{MAX}} \left| \frac{\partial T}{\partial x} \right| \right) \,. \tag{2}$$

We then assume that, over a certain value of tracer gradient $\frac{\partial T}{\partial x}_{MAX}$, the fish are able to climb the gradient without being affected by the noise. This assumption, from a biological perspective, means that the fish does not live in a completely noisy environment, but that under favorable circumstances it is able to correctly identify the swimming direction. This means that

$$f_W * \frac{\partial T}{\partial x}_{MAX} = \xi_{MAX} \,. \tag{3}$$

Substituting then (3) into (2) gives:

$$U_F(x) = V \frac{\frac{\partial T}{\partial x}}{\frac{\partial T}{\partial x}_{MAX}} \left(2 - \frac{\left| \frac{\partial T}{\partial x} \right|}{\frac{\partial T}{\partial x}_{MAX}} \right) \,. \tag{4}$$

507   Finally, we can include an eventual effect of currents speed, considering that
508   the tracer is transported passively by them, simply adding the current speed U_C
509   to Expr. (4).
510   The representations provided are individual based, with each individual repre-
511   senting a single fish. However, we note that all the considerations done are also
512   valid if we consider an individual representing a fish school. U_F will then simply
513   represent the average velocity of the fish schools. This aspect should be stressed
514   since many fish species live and feed in groups (see SI.2 for further details).
515   **Continuity equation in one dimension.** The solution of this model will now
516   be discussed. The continuity equation is first considered in one dimension. The
517   starting scenario is simply an initially homogeneous distribution of fish, that are
518   moving in a one dimensional space with a velocity given by $U_F(x)$.
519   We assume that in the time scales considered (few days to some weeks), the
520   fish biomass is conserved, so for instance fishing mortality or growing rates are
521   neglected. In that case, we can express the evolution of the concentration of the
522   fish ρ by the continuity equation

$$\frac{\partial \rho}{\partial t} + \nabla \cdot \mathbf{j} = 0 \tag{5}$$

523   in which $\mathbf{j} = \rho \, U_F(x)$, so that Eq. (5) becomes

$$\frac{\partial \rho}{\partial t} + \nabla \cdot \left(\rho \, U_F(x) \right) = 0 \; . \tag{6}$$

524   In one dimension, the divergence is simply the partial derivate along the x-axis.
525   Eq. (6) becomes

$$\frac{\partial \rho}{\partial t} = -\frac{\partial}{\partial x} \left(\rho \, U_F \right) \tag{7}$$

526   Now, we decompose the fish concentration ρ in two parts, a constant one and a
527   variable one $\rho = \rho_0 + \tilde{\rho}$. Eq. (7) will then become

$$\frac{\partial \rho}{\partial t} = -U_F \frac{\partial \tilde{\rho}}{\partial x} - \rho \frac{\partial U_F}{\partial x} \; . \tag{8}$$

528   Using Expr. (4), Eq. (8) is numerically simulated with the Lax method. In
529   Expr. (4) we impose that $U_F(x) = V$ when $U_F(x) > V$. This biological assump-
530   tion means that fish maximal velocity is limited by a physiological constraint
531   rather than by gradient steepness. Details of the physical and biological param-
532   eters are provided in SI.5.

Acknowledgements

16   Fine-scale fronts as hotspots of fish aggregation in the open ocean.

543   Authors contribution

544   A.B., E.S.G. and F.d.O designed the research with assistance from X.C. A.B.
545   performed the research. A.B. and D.d.O. analyzed the data. C.C. and Y.C.
546   provided the data. A.B. wrote the paper, with assistance from F.d.O., E.S.G,
547   D.d.O, X.C., and C.C.

Bibliography

Abrahms, B., Scales, K.L., Hazen, E.L., Bograd, S.J., Schick, R.S., Robinson, P.W., Costa, D.P., 2018. Mesoscale activity facilitates energy gain in a top predator. Proc. R. Soc. B, 285:20181101. doi:10.1098/rspb.2018.1101.

Adler, J., 1975. Chemotaxis in bacteria. Annual review of biochemistry, 44:341–356.

Alonzo, F., Mayzaud, P., Razouls, S., Bocher, P., Cherel, Y., 2003. Seasonal changes in biomass, growth rates and production of subantarctic calanoid copepods in the Bay of Morbihan, Kerguelen Islands. Marine Biology, 142:525–536. doi:10.1007/s00227-002-0976-5.

Béhagle, N., Cotté, C., Lebourges-Dhaussy, A., Roudaut, G., Duhamel, G., Brehmer, P., Josse, E., Cherel, Y., 2017. Acoustic distribution of discriminated micronektonic organisms from a bi-frequency processing: The case study of eastern Kerguelen oceanic waters. Progress in Oceanography, 156:276 – 289. doi:https://doi.org/10.1016/j.pocean.2017.06.004.

Bertrand, A., Grados, D., Colas, F., Bertrand, S., Capet, X., Chaigneau, A., Vargas, G., Mousseigne, A., Fablet, R., 2014. Broad impacts of fine-scale dynamics on seascape structure from zooplankton to seabirds. Nature Communications, 5:5239. doi:10.1038/ncomms6239.

Boffetta, G., Lacorata, G., Redaelli, G., Vulpiani, A., 2001. Detecting barriers to transport: a review of different techniques. Physica D: Nonlinear Phenomena, 159:58–70. doi:10.1016/S0167-2789(01)00330-X.

Cherel, Y., Fontaine, C., Richard, P., Labatc, J.P., 2010. Isotopic niches and trophic levels of myctophid fishes and their predators in the southern ocean. Limnology and oceanography, 55:324–332.

De Monte, S., Cotté, C., d'Ovidio, F., Lévy, M., Le Corre, M., Weimerskirch, H., 2012. Frigatebird behaviour at the ocean–atmosphere interface: integrating animal behaviour with multi-satellite data. Journal of The Royal Society Interface, 9:3351–3358. doi:10.1098/rsif.2012.0509.

De Monte, S., Soccodato, A., Alvain, S., d'Ovidio, F., 2013. Can we detect oceanic biodiversity hotspots from space? The ISME journal, 7:2054. doi:10.1038/ismej.2013.72.

Della Penna, A., De Monte, S., Kestenare, E., Guinet, C., d'Ovidio, F., 2015. Quasi-planktonic behavior of foraging top marine predators. Scientific reports, 5. doi:10.1038/srep18063.

d'Ovidio, F., De Monte, S., Della Penna, A., Cotté, C., Guinet, C., 2013. Ecological implications of eddy retention in the open ocean: a Lagrangian approach. Journal of Physics A: Mathematical and Theoretical, 46:254023. doi:10.1088/1751-8113/46/25/254023.

d'Ovidio, F., Fernández, V., Hernández-García, E., López, C., 2004. Mixing structures in the Mediterranean Sea from finite-size Lyapunov exponents. Geophysical Research Letters, 31. doi:10.1029/2004GL020328.

d'Ovidio, F., Monte, S.D., Alvain, S., Dandonneau, Y., Lévy, M., 2010. Fluid dynamical niches of phytoplankton types. Proceedings of the National Academy of Sciences, 107:18366–18370. doi:10.1073/pnas.1004620107.

Duhamel, G., Hulley, P.A., Causse, R., Koubbi, P., Vacchi, M., Pruvost, P., Vigetta, S., Irisson, J.O., Mormède, S.A.B.M., Dettai, A.A.D.H.W.A.G.J.A.J.C.D., Kock, K.H., Lopez Abellan, L.J., Van de Putte, A.P., 2014. Biogeographic Patterns Of Fish (Biogeographic Atlas of the Southern Ocean), chapter Biogeographic Patterns Of Fish, pages 328–362. Scientific Committee on Antarctic Research, Cambridge UK.

Gaines, S.D., White, C., Carr, M.H., Palumbi, S.R., 2010. Designing marine reserve networks for both conservation and fisheries management. Proceedings of the National Academy of Sciences. doi:10.1073/pnas.0906473107.

Genin, A., Jaffe, J.S., Reef, R., Richter, C., Franks, P.J.S., 2005. Swimming Against the Flow: A Mechanism of Zooplankton Aggregation. Science, 308:860–862. doi:10.1126/science.1107834.

Greely, T.M., Gartner Jr, J.V., Torres, J.J., 1999. Age and growth of Electrona antarctica (Pisces: Myctophidae), the dominant mesopelagic fish of the Southern Ocean. Marine Biology, 133:145–158. doi:10.1007/s002270050453.

Haller, G., 2015. Lagrangian coherent structures. Annual Review of Fluid Mechanics, 47:137–162. doi:10.1146/annurev-fluid-010313-141322.

Hoegh-Guldberg, O., Bruno, J.F., 2010. The Impact of Climate Change on the World's Marine Ecosystems. Science, 328:1523–1528. doi:10.1126/science.1189930.

Irigoien, X., Klevjer, T.A., Røstad, A., Martinez, U., Boyra, G., Acuña, J., Bode, A., Echevarria, F., Gonzalez-Gordillo, J., Hernandez-Leon, S., et al., 2014. Large mesopelagic fishes biomass and trophic efficiency in the open ocean. Nature communications, 5. doi:dx.doi.org/10.1038/ncomms4271.

Kai, E.T., Rossi, V., Sudre, J., Weimerskirch, H., Lopez, C., Hernandez-Garcia, E., Marsac, F., Garcon, V., 2009. Top marine predators track lagrangian coherent structures. Proceedings of the National Academy of Sciences of the United States of America, 106:8245–8250. doi:10.1073/pnas.0811034106.

Kasumyan, A., 2004. The olfactory system in fish: structure, function, and role in behavior. Journal of Ichthyology, 44:S180.

Kloser, R.J., Ryan, T.E., Young, J.W., Lewis, M.E., 2009. Acoustic observations of micronekton fish on the scale of an ocean basin: potential and challenges. ICES Journal of Marine Science, 66:998–1006. doi:10.1093/icesjms/fsp077.

Koenker, R., 2005. Quantile Regression. Econometric Society Monographs. Cambridge University Press. doi:10.1017/CBO9780511754098.

Koubbi, P., Moteki, M., Duhamel, G., Goarant, A., Hulley, P.A., ODriscoll, R., Ishimaru, T., Pruvost, P., Tavernier, E., Hosie, G., 2011. Ecoregionalization of myctophid fish in the Indian sector of the Southern Ocean: Results from generalized dissimilarity models. Deep Sea Research Part II: Topical Studies in Oceanography, 58:170 – 180. doi:https://doi.org/10.1016/j.dsr2.2010.09.007. Census of Antarctic Marine Life: Diversity and Change in the Southern Ocean Ecosystems.

635 Kwon, E.Y., Primeau, F., Sarmiento, J.L., 2009. The impact of remineralization
636   depth on the air–sea carbon balance. Nature Geoscience, 2:630.

637 Labat, J.P., Mayzaud, P., Sabini, S., 2005. Population dynamics of Themisto
638   gaudichaudii in Kerguelen Islands waters, Southern Indian Ocean. Polar Bi-
639   ology, 28:776–783. doi:10.1007/s00300-005-0003-7.

640 Lara-Lopez, A.L., Davison, P., Koslow, J.A., 2012. Abundance and community
641   composition of micronekton across a front off Southern California. Journal of
642   Plankton Research, 34:828–848. doi:10.1093/plankt/fbs016.

643 Lehahn, Y., d'Ovidio, F., Koren, I., 2018. A satellite-based lagrangian view
644   on phytoplankton dynamics. Annual Review of Marine Science, 10:99–119.
645   doi:10.1146/annurev-marine-121916-063204. PMID: 28961072.

646 Lévy, M., Franks, P.J.S., Smith, K.S., 2018. The role of submesoscale currents
647   in structuring marine ecosystems. Nature Communications, 9. doi:10.1038/
648   s41467-018-07059-3.

649 Lévy, M., Martin, A.P., 2013. The influence of mesoscale and submesoscale het-
650   erogeneity on ocean biogeochemical reactions. Global Biogeochemical Cycles,
651   27:1139–1150. doi:10.1002/2012GB004518.

652 Martin, A., 2003. Phytoplankton patchiness: the role of lateral stirring and
653   mixing. Progress in Oceanography, 57:125 – 174. doi:https://doi.org/10.1016/
654   S0079-6611(03)00085-5.

655 McGillicuddy, D.J., 2016. Mechanisms of Physical-Biological-Biogeochemical In-
656   teraction at the Oceanic Mesoscale. Annual Review of Marine Science, 8:125–
657   159. doi:10.1146/annurev-marine-010814-015606. PMID: 26359818.

658 McManus, M.A., Woodson, C.B., 2012. Plankton distribution and ocean disper-
659   sal. Journal of Experimental Biology, 215:1008–1016. doi:10.1242/jeb.059014.

660 Morrow, R., Fu, L.L., Ardhuin, F., Benkiran, M., Chapron, B., Cosme, E.,
661   D'Ovidio, F., Farrar, J.T., Gille, S.T., Lapeyre, G., et al., 2019. Global ob-
662   servations of fine-scale ocean surface topography with the surface water and
663   ocean topography (swot) mission. Frontiers in Marine Science, 6:232.

664 Netburn, A.N., Koslow, J.A., 2018. Mesopelagic fish assemblages across oceanic
665   fronts: A comparison of three frontal systems in the southern California Cur-
666   rent Ecosystem. Deep Sea Research Part I: Oceanographic Research Papers,
667   134:80 – 91. doi:https://doi.org/10.1016/j.dsr.2018.03.005.

668 Ohman, M.D., 1988. Sources of variability in measurements of copepod lipids
669   and gut fluorescence in the california current coastal zone. Marine Ecology
670   Progress Series, 42:143–153.

671 Pakhomov, E., Perissinotto, R., McQuaid, C., 1996. Prey composition and daily
672   rations of myctophid fishes in the southern ocean. Marine Ecology Progress
673   Series, pages 1–14.

674 Pakhomov, E.A., Froneman, P.W., 2000. Composition and spatial variability
675   of macroplankton and micronekton within the Antarctic Polar Frontal Zone
676   of the Indian Ocean during austral autumn 1997. Polar Biology, 23:410–419.
677   doi:10.1007/s003000050462.

678 PC, E.F., RL, O., JC, M., 2018. Predicting distribution and relative abun-
679   dance of mid-trophic level organisms using oceanographic parameters and

acoustic backscatter. Marine Ecology Progress Series, 592:37–56. doi: 10.3354/meps12519.

Penna, A.D., Koubbi, P., Cott, C., Bon, C., Bost, C.A., d'Ovidio, F., 2017. Lagrangian analysis of multi-satellite data in support of open ocean Marine Protected Area design. Deep Sea Research Part II: Topical Studies in Oceanography, 140:212 – 221. doi:https://doi.org/10.1016/j.dsr2.2016.12.014. Future of oceanic animals in a changing ocean.

Prants, S., Budyansky, M., Uleysky, M., 2014. Identifying Lagrangian fronts with favourable fishery conditions. Deep Sea Research Part I: Oceanographic Research Papers, 90:27 – 35. doi:https://doi.org/10.1016/j.dsr.2014.04.012.

Robinson, L.M., Elith, J., Hobday, A.J., Pearson, R.G., Kendall, B.E., Possingham, H.P., Richardson, A.J., 2011. Pushing the limits in marine species distribution modelling: lessons from the land present challenges and opportunities. Global Ecology and Biogeography, 20:789–802. doi:10.1111/j.1466-8238.2010.00636.x.

Sankaran, M., Hanan, N.P., Scholes, R.J., Ratnam, J., Augustine, D.J., Cade, B.S., Gignoux, J., Higgins, S.I., Le Roux, X., Ludwig, F., et al., 2005. Determinants of woody cover in African savannas. Nature, 438:846. doi: 10.1038/nature04070.

Sato, M., Barth, J.A., Benoit-Bird, K.J., Pierce, S.D., Cowles, T.J., Brodeur, R.D., Peterson, W.T., 2018. Coastal upwelling fronts as a boundary for planktivorous fish distributions. Marine Ecology Progress Series, 595:171–186. doi: 10.3354/meps12553.

Saunders, R.A., Fielding, S., Thorpe, S.E., Tarling, G.A., 2013. School characteristics of mesopelagic fish at South Georgia. Deep Sea Research Part I: Oceanographic Research Papers, 81:62 – 77. doi:https://doi.org/10.1016/j.dsr.2013.07.007.

Scales, K.L., Hazen, E.L., Jacox, M.G., Castruccio, F., Maxwell, S.M., Lewison, R.L., Bograd, S.J., 2018. Fisheries bycatch risk to marine megafauna is intensified in Lagrangian coherent structures. Proceedings of the National Academy of Sciences of the United States of America. doi:10.1073/pnas.1801270115.

Snyder, S., Franks, P.J.S., Talley, L.D., Xu, Y., Kohin, S., 2017. Crossing the line: Tunas actively exploit submesoscale fronts to enhance foraging success. Limnology and Oceanography Letters, 2:187–194. doi:10.1002/lol2.10049.

St. John, M.A., Borja, A., Chust, G., Heath, M., Grigorov, I., Mariani, P., Martin, A.P., Santos, R.S., 2016. A Dark Hole in Our Understanding of Marine Ecosystems and Their Services: Perspectives from the Mesopelagic Community. Frontiers in Marine Science, 3:31. doi:10.3389/fmars.2016.00031.

Sulman, M.H., Huntley, H.S., Lipphardt, B., Kirwan, A., 2013. Leaving flatland: Diagnostics for Lagrangian coherent structures in three-dimensional flows. Physica D: Nonlinear Phenomena, 258:77 – 92. doi:https://doi.org/10.1016/j.physd.2013.05.005.

Sutton, T.T., Clark, M.R., Dunn, D.C., Halpin, P.N., Rogers, A.D., Guinotte, J., Bograd, S.J., Angel, M.V., Perez, J.A.A., Wishner, K., Haedrich, R.L., Lindsay, D.J., Drazen, J.C., Vereshchaka, A., Piatkowski, U., Morato, T., Bachowiak-Samoyk, K., Robison, B.H., Gjerde, K.M., Pierrot-Bults, A.,

726   Bernal, P., Reygondeau, G., Heino, M., 2017. A global biogeographic clas-
727   sification of the mesopelagic zone. Deep Sea Research Part I: Oceanographic
728   Research Papers, 126:85 – 102. doi:https://doi.org/10.1016/j.dsr.2017.05.006.
729   Vidal, J., 1980. Physioecology of zooplankton. I. Effects of phytoplankton con-
730   centration, temperature, and body size on the growth rate of Calanus pacificus
731   and Pseudocalanus sp. Marine Biology, 56:111–134. doi:10.1007/BF00397129.
732   Watson, J.R., Fuller, E.C., Castruccio, F.S., Samhouri, J.F., 2018. Fishermen
733   Follow Fine-Scale Physical Ocean Features for Finance. Frontiers in Marine
734   Science, 5. doi:10.3389/fmars.2018.00046.
735   Woodson, C.B., Litvin, S.Y., 2015. Ocean fronts drive marine fishery production
736   and biogeochemical cycling. Proceedings of the National Academy of Sciences,
737   112:1710–1715. doi:10.1073/pnas.1417143112.
738   Yoder, J.A., Ackleson, S.G., Barber, R.T., Flament, P., Balch, W.M., 1994. A
739   line in the sea. Nature, 371:689. doi:10.1038/371689a0.